Intermediate-valent CeCoAl - a commensurate modulated structure with short Ce-Co distances

Oliver Niehaus, Rolf-Dieter Hoffmann, Sophie Tencé, Bernard Chevalier, Rainer Pöttgen

Oliver Niehaus, Rolf-Dieter Hoffmann, Sophie Tencé, Bernard Chevalier and Rainer Pöttgen*

Intermediate-valent CeCoAl – a commensurate modulated structure with short Ce–Co distances

DOI 10.1515/zkri-2015-1856
Received April 30, 2015; accepted June 11, 2015; published online July 4, 2015

Abstract: CeCoAl was synthesized by melting of the elements in a sealed niobium tube in an induction furnace. Annealing of the sample gave access to a single phase sample. Its structure was refined on the basis of single-crystal X-ray diffractometer data at different temperatures. Above 271 K CeCoAl crystallizes in its own structure type in the space group $C2/m$ [a = 1107.4(2), b = 440.6(1) and c = 479.6(1) pm, β = 104.6(1)°]. Data obtained at 300 K lead to 511 F^2 values with 20 variables and a residual of [I ≥ 3σ(I)] wR = 0.0539. Below 271 K satellites give rise to the superspace group $C2/m(\alpha 0 \gamma)00$; α = 2/3, γ = 2/5 with a temperature independent q-vector. For the 90 K data (also for 180 and 220 K) the commensurate modulated structure could be refined with 4817 F^2 values, 129 variables and residuals of wR = 0.0347 (main), wR = 0.1927 (satellites 1st order), wR = 0.1541 (satellites 2nd order) and wR = 0.1768 (satellites 3rd order) [a = 1107.5(1), b = 440.3(1) and c = 479.0(1) pm, β = 104.7(1)°]. For the three temperatures only minor variations of the modulation amplitudes are observed. The relation of the low temperature (3+1)D $3a \times 5c$ approximant and the room temperature 3D structure is discussed on the basis of a group–subgroup relation. By investigation of the heat capacity, the phase transition could be identified as a second order one with a transition temperature of 271 K. Magnetic measurements clearly prove the intermediate cerium valence which is in line with the short Ce–Co distances.

Keywords: cerium; group-subgroup scheme; intermediate valence compound; modulated structure.

***Corresponding author: Rainer Pöttgen,** Institut für Anorganische und Analytische Chemie, Universität Münster, Corrensstrasse 30, 48149 Münster, Germany, E-mail: pottgen@uni-muenster.de
Oliver Niehaus and Rolf-Dieter Hoffmann: Institut für Anorganische und Analytische Chemie, Universität Münster, Corrensstrasse 30, 48149 Münster, Germany
Sophie Tencé and Bernard Chevalier: CNRS, Université de Bordeaux, ICMCB, UPR 9048, F-33600 Pessac, France

Introduction

Among the large number of equiatomic CeTX intermetallics (T = electron-rich transition metal; X = element of the 3rd, 4th or 5th main group) [1–5], CeCoAl [6–14], CeCoGa [6, 15–17], and CeRuSn [18–29] exhibit unusual crystal chemistry. These three intermetallics have the same valence electron count and the same subcell structure which derives from the Bi_2Pd type [30–32], space group $C2/m$, through an ordering of the cerium and aluminum (gallium, tin) atoms on the bismuth sites. Nevertheless, the structural chemistry of these three intermetallics is much more complex than expected from the simple comparison with Bi_2Pd.

Temperature-dependent diffraction data were so far only reported for CeRuSn. The first study [18] revealed the ordered Bi_2Pd type subcell structure with space group $C2/m$, however, with extreme anisotropic displacements for the ruthenium atoms. Room temperature single crystal data revealed a doubling of the subcell along the c-axis and commensurate superstructure formation through an isomorphic transition of index 2 ($i2$). This study revealed an ordering of trivalent and intermediate valence cerium atoms along with extremely short Ce–Ru distances for the almost tetravalent cerium atoms. At lower temperatures modulations occurred and the nuclear structure was described within the superspace formalism in (3+1) dimensions. The nuclear modulation vector showed a strong initial temperature dependence and then tends towards a value close to q = (0 0 0.35). These structural changes go along with changes in the magnetic and transport behaviors (R.-D. Hoffmann et al., unpublished results).

The remarkable structural behavior and the outstanding physical properties of CeRuSn drew our attention to the structurally closely related phases CeCoAl and CeCoGa, since first property studies also revealed intermediate cerium valence. While the gallide was characterized only on the basis of powder diffraction data [7, 17], a single crystal structure refinement was reported for CeCoAl [7]. The refinement results showed the same anomaly as the subcell refinement for CeRuSn [18], i.e. a significant displacement of the cobalt atoms along the c-axis.

In continuation of our structural studies on CeRuSn, we synthesized well-shaped single crystals of CeCoAl and studied their structures from high-resolution diffraction data as a function of temperature. The structure and properties of CeCoAl are reported herein. CeCoGa shows a complex commensurate modulation already at room temperature and will be described in a separate publication.

Experimental

Synthesis

Starting materials for the synthesis of CeCoAl were ingots of cerium (Sigma-Aldrich), cobalt powder (Koch chemicals, >99.5 %) and aluminum turnings (Koch chemicals), except of Co all with stated purities of 99.9 % or higher. The air- and moisture-sensitive cerium ingots were kept in Schlenk tubes under argon prior to the reaction. The elements were weighed in the ideal 1:1:1 atomic ratio and arc-welded [33] in a niobium tube under 800 mbar argon. Argon was purified with titanium sponge (900 K), silica gel, and molecular sieves. The niobium ampoule was subsequently placed in the water-cooled sample chamber of an induction furnace (Hüttinger Elektronik, Freiburg, Germany, Typ TIG 1.5/300) [34] and heated under a steady flow of argon to ~1500 K. To obtain high quality single crystals this temperature was kept for 10 min and then slowly lowered by 5–10 K/min to 900 K. The sample was quenched after the annealing process of about 6 h by switching off the power supply. As temperature control unit a Metis MS09 (Sensortherm) pyrometer (accuracy ± 50 K) was used. To enhance the purity of the sample a cold-pressed pellet (∅ 6 mm) of the reaction product was annealed for further 4 weeks in an evacuated silica ampoule at 770 K. The polycrystalline sample showed metallic luster, while the powder is dark gray. No reactions with the ampoule material were observed. The compound is stable in air over months.

Alternatively the sample can be prepared by melting precisely weighed amounts of high purity elements in a levitation furnace. Melting was carried out in a water-cooled copper crucible under a purified argon atmosphere and repeated several times to achieve good homogeneity. Annealing was done for one month at 923 K by enclosing this sample in an evacuated quartz tube. No reaction between the tube and the sample was observed. The sample quality of the arc-melting and the levitation melting experiment was similar.

X-ray diffraction

The polycrystalline CeCoAl sample was characterized by powder X-ray diffraction on a Guinier camera (equipped with an image plate system Fujifilm, BAS-1800) using Cu $K_{\alpha 1}$ radiation and α-quartz (a = 491.30 and c = 540.46 pm) as an internal standard. The monoclinic lattice parameters (Table 1) were obtained from a least-squares fit. Proper indexing of the diffraction lines was ensured by an intensity calculation [35] using the positional parameters obtained from the single crystal investigation (subcell data). The powder and single crystal lattice parameters showed good agreement with values from literature [7]. The experimental and simulated ($C2/m$ subcell data) powder pattern is presented in Figure 1. The sample was pure on the level of X-ray powder diffraction. X-ray fluorescence (a cobalt containing sample measured with copper radiation) hampered a more detailed analyses of the pattern.

Crystal fragments were obtained from the crushed CeCoAl sample. The crystals were glued to quartz fibres using bees wax and their quality for intensity data collection was checked by Laue photographs on a Buerger camera (white molybdenum radiation, image plate technique, Fujifilm, BAS-1800). The data set was measured on a Stoe StadiVari diffractometer equipped with a Mo micro focus source and a Pilatus detection system and scaled subsequently due to the Gaussian-shaped profile of the X-ray source. Numerical absorption corrections (along with scaling for the StadiVari data set) were applied to the data sets. All relevant crystallographic data and details of the data collection and evaluation are listed in Table 1.

EDX analysis

The single crystal investigated on the diffractometer was studied by semiquantitative EDX analyses using a Zeiss EVO® MA10 scanning electron microscope in variable pressure mode with CeO_2, Co, and Al_2O_3 as standards. The analysis at several points of the crystal is in line with the equiatomic stoichiometry. No impurity elements (especially from the container material) were observed.

Physical property studies

Magnetic susceptibility and heat capacity investigations have been performed in a Quantum Design physical-property-measurement-system (PPMS) using a vibrating sample magnetometer (VSM) and the heat capacity option, respectively.

For the VSM measurement 12.0 mg of the powdered sample was packed in a polypropylene capsule and attached to the sample holder rod. The sample was investigated in the temperature range of 2.5–305 K with magnetic flux densities up to 80 kOe. For the heat capacity measurements, a 1.276 mg piece of the sintered tablet was fixed to a pre-calibrated heat capacity puck using Apiezon N grease and investigated in a similar temperature range like the magnetic investigations.

Structure refinement

Careful analyses of the diffractometer data set at 300 K revealed a C-centrered monoclinic lattice and the systematic extinctions were compatible with the space group $C2/m$. The starting atomic parameters were deduced using the charge-flipping algorithm of Superflip [36] and the CeCoAl structure was refined with anisotropic

Tab. 1: Crystallographic data and structure refinement of the ambient and low temperatures data sets for CeCoAl; superspace group $C2/m(\alpha 0\gamma)00$ with $q = 2/3, 0, 2/5$; $Z = 4$.

Empirical formula	CeCoAl			
Formula weight/g mol^{-1}	226.0			
Unit cell dimensions/pm	$a = 1109.3(1)$			
(Guinier powder data at room temperature)	$b = 441.1(1)$			
	$c = 480.5(1)$			
	$\beta = 104.6(1)$			
Cell volume/nm^3	0.2275			
Crystal size/µm^3	$80 \times 40 \times 30$			
Diffractometer type	StadiVari			
Wave length/pm	71.073 (MoK$_\alpha$)			
Temperature/K	300	220	180	90
Calculated density/g cm^{-3}	6.63	6.62	6.63	6.64
Unit cell dimensions/pm	$a = 1107.4(2)$	$a = 1108.3(1)$	$a = 1107.9(1)$	$a = 1107.5(1)$
	$b = 440.6(1)$	$b = 440.7(1)$	$b = 440.5(1)$	$b = 440.3(1)$
	$c = 479.6(1)$	$c = 479.6(1)$	$c = 479.4(1)$	$c = 479.0(1)$
	$\beta = 104.6(1)$	$\beta = 104.6(1)$	$\beta = 104.6(1)$	$\beta = 104.7(1)$
Volume/nm^3	0.2264	0.2267	0.2265	0.2259
Detector distance/mm	40	40	40	40
Exposure time/sec	8	58	40	60
Integrated parameter (A, B, EMS)	8.0, −6.0, 0.030	5.0, −3.0, 0.030	4.0, −2.0, 0.020	6.0, −3.0, 0.030
Satellite profile factor		0.6	0.8	0.6
Absorption coefficient/mm^{-1}	27.1	28.1	27.1	27.2
Transm. ratio (max/min)	0.79/0.5	0.79/0.5	0.79/0.5	0.79/0.5
F(000)/e	392	392	392	392
θ range for data collection/°	3.8–34	2.5–39.5	2.5–39.1	2.5–38.9
Range in *hkl*	±17, ±6, ±7	±20, ±7, ±9	±20, ±7, ±9	±20, ±7, ±9
Total no. reflections	3512	27,356	25,930	22,955
Independent reflections/R_{int}	511/0.0846	5009/0.0520	4970/0.0619	4817/0.0579
Reflections with $I \geq 3\sigma(I)$	337/0.1034	1415/0.0324	1223/0.0534	1427/0.0501
Main + Satellite (1st, 2nd, 3rd)	–	641 + 114 + 260 + 208	658 + 180 + 337 + 240	602 + 160 + 355 + 310
Data/parameters	511/20	5009/129	4970/129	4817/129
Goodness-of-fit on F^2	0.65	0.95	0.92	0.94
$R1/wR2$ for $I \geq 3\sigma(I)$	0.0281/0.0539	0.0272/0.0545	0.0301/0.0556	0.0306/0.0588
Main		0.0167/0.0411	0.0192/0.0442	0.0158/0.0347
Satellites 1st order		0.0694/0.1510	0.0764/0.1699	0.0810/0.1927
Satellites 2nd order		0.0730/0.1573	0.0785/0.1661	0.0733/0.1541
Satellites 3rd order		0.0930/0.1863	0.0895/0.1917	0.0852/0.1768
$R1/wR2$ (all data)	0.0453/0.0573	0.1103/0.0730	0.1363/0.0775	0.1280/0.0775
Main		0.0190/0.0416	0.0224/0.0483	0.0191/0.0355
Satellites 1st order		0.3812/0.3281	0.4167/0.3913	0.3917/0.3771
Satellites 2nd order		0.2540/0.2228	0.2924/0.2608	0.2535/0.2225
Satellites 3rd order		0.3191/0.2798	0.3335/0.2909	0.2738/0.2374
Extinction coefficient	218(11)	120(7)	107(7)	71(7)
Largest diff. peak/hole, /e Å^{-3}	0.68/ −0.55	3.54/ −5.02	2.78/ −3.08	4.64/ −6.55

displacement parameters for all atoms with Jana2006 [37]. As a check for the correct composition and site assignment the occupancy parameters were refined in separate series of least-squares cycles. All sites were fully occupied within three standard deviations. The final difference electron-density synthesis was flat. Details of the refinement and the positional parameters are listed in Tables 1 and 2. Table 3 lists the distances within the room temperature structure. Further information on the structure refinement is available.[1]

1 Details may be obtained from: Fachinformationszentrum Karlsruhe, D-76344 Eggenstein-Leopoldshafen (Germany), by quoting the Registry No's. CSD–429552 (300 K data), CSD–429553 (220 K data), CSD–429554 (180 K data) and CSD–429555 (90 K data).

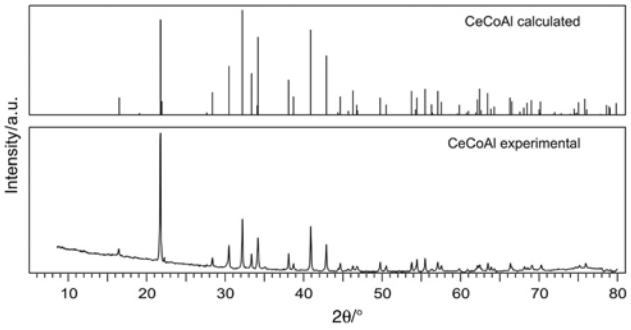

Fig. 1: Experimental and simulated (*C*2/*m* subcell data) Guinier powder patterns (Cu $K\alpha_1$ radiation) for CeCoAl.

Except of a slightly enhanced U_{33} (approx. $3 \times U_{22}$) parameter of 418 pm² for the Co-site no structural anomalies can be observed (cp. Figure 2). Due to our experiences with CeRuSn (*vide supra*) we performed X-ray single crystal investigations at temperatures below 300 K. Like demonstrated in Figure 3 already at 220 K a sufficient amount of additional reflections can be observed along *a** as well as *c** in comparison to the 300 K measurement. Systematic extinctions exclude a simple multiplication of the *a*- and *c*-axis as well as a (3+2)D modulated structure with *q*-vectors for both mentioned axes. Only six of the possible 14 satellites for a *C*-centered $3a \times 5c$ approximant structure can be regularly observed (orange lattice, Figure 3). This situation leads to a description of LT-CeCoAl as (3+1)D commensurate modulated superstructure in the space group $C2/m(\alpha 0\gamma)00$ with $q = (2/3, 0, 2/5)$. The *q*-vector is symbolized in Figure 3 by black arrows and clearly shows the existence of satellites up to 3rd order, drawn as blue pentagons.

The structure solution again was performed with Superflip [36] and the refinement on F^2 with Jana2006 [37]. An additional scale factor was applied to the satellite reflections accommodating the many possible antiphase boundaries due to the occurring isomorphic symmetry reduction (*vide infra*), which significantly improved the residuals of the refinement. To some extent this scaling problem might also originate from the integration and scaling procedure while processing the micro source raw data. Note, the weak intensities of satellite reflections are indeed in the order of the Laue streaks of strong main reflections due to long employed counting times. Therefore, main reflections are integrated with sufficient large areas, while for the satellites a smaller area is applied with a profile factor less than one. For all three positions harmonic modulations up to third order were applied. Furthermore it was possible to refine modulated atomic displacement parameters (ADP) up to the third order, again for all atoms. The commensurate option was used with a $3a \times 5c$ supercell, $t_0 = 1/(2N) = 1/(2(3 \times 5)) = 1/30$ and *C*2/*m* for the approximant. A $t_0 = 0$ is not reasonable – it leads to a disordered approximant. At 90 K, the corresponding description of the atom domains is depicted in Figure 4 and the values are listed in Table 4. Slight position modulations can be observed for all atoms along the *a*-axis and for Ce and Al along the *c*-axis. In accordance to the slightly enhanced U_{33} value of Co in the subcell, the most distinct position modulation is observed for Co along the *c*-axis. As a check for the correct composition, the occupancy parameters were refined in a separate series of least-squares cycles. Also for the temperatures below the phase transition all sites are fully occupied within three standard deviations. The final difference electron-density synthesis was flat. Details of the refinements are also listed in Table 1.

The group-subgroup relation in the Bärnighausen formalism [38–41] for the 3D and (3+1)D space groups is presented in Figure 5. To be able to project the commensurate modulated structure onto 3D space an approximant structure has to be chosen. Therefore, the lattice parameters of the basic structure have to be multiplied by the denominators of the *q*-vectors. For LT-CeCoAl the smallest approximant supercell is realized by 3*a* and 5*c*. Both transformations are classified as *isomorphic*. For the transformation from the (3+1)D space group to the approximant structure an index *a* has already been introduced in literature [42]. The index of this transformation is *a*15 due to symmetry thinning by the corresponding factors (*vide infra*). Because of the possibility to describe the modulation as a commensurate one, no difference referring to the atom sites with

Tab. 2: Atom positions and anisotropic displacement parameters (pm²) of CeCoAl at 300 K.

Atom	Wyckoff site	*x*	*y*	*z*	U_{11}	U_{22}	U_{33}	U_{13}	U_{eq}
Ce	4*i*	0.12966(7)	0	0.32455(14)	168(3)	149(3)	132(2)	42(2)	149(2)
Co	4*i*	0.19302(15)	0	0.8516(4)	186(7)	136(7)	418(10)	80(7)	246(5)
Al	4*i*	0.4144(3)	0	0.1895(7)	188(14)	138(12)	185(14)	78(12)	165(8)

U_{eq} is defined as one third of the trace of the orthogonalized U_{ij} tensor. Coefficients U_{ij} of the anisotropic displacement factor tensor of the atoms are defined by: $-2\pi^2[(ha^*)^2U_{11} + \ldots + 2hka^*b^*U_{12}]$. $U_{12} = U_{23} = 0$.

Tab. 3: Interatomic distances (pm) for CeCoAl at 300 K.

Atom1	#	Atom2	Distance
Ce:	1	Co	244.7
	1	Co	253.8
	2	Al	319.0
	2	Co	320.3
	2	Al	325.0
	2	Al	333.1
	1	Al	337.5
	1	Co	345.8
	2	Ce	353.9
	1	Ce	366.4
	1	Ce	367.7
Co:	1	Ce	244.7
	2	Al	248.8
	1	Ce	253.8
	1	Al	257.5
	2	Co	275.0
	2	Ce	320.3
	1	Ce	345.8
Al:	2	Co	248.8
	1	Co	257.5
	1	Al	293.9
	1	Al	310.1
	2	Ce	319.0
	2	Ce	325.0
	2	Ce	333.1
	1	Ce	337.5

Standard deviations are equal or smaller than 0.5 pm.

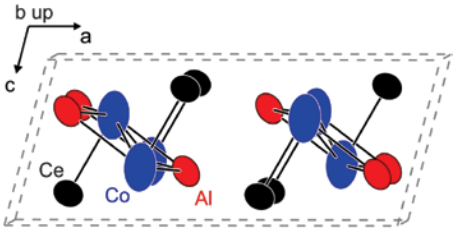

Fig. 2: Crystal structure of CeCoAl at 300 K. Cerium, cobalt and aluminum atoms are drawn as black, blue, and red circles, respectively (displacement ellipsoids at 99 % probability). Note, for drawing purposes a shift of 1/2 0 1/2 as allowed by the Euclidian normalizer has been applied as compared to Table 2 and Figure 5.

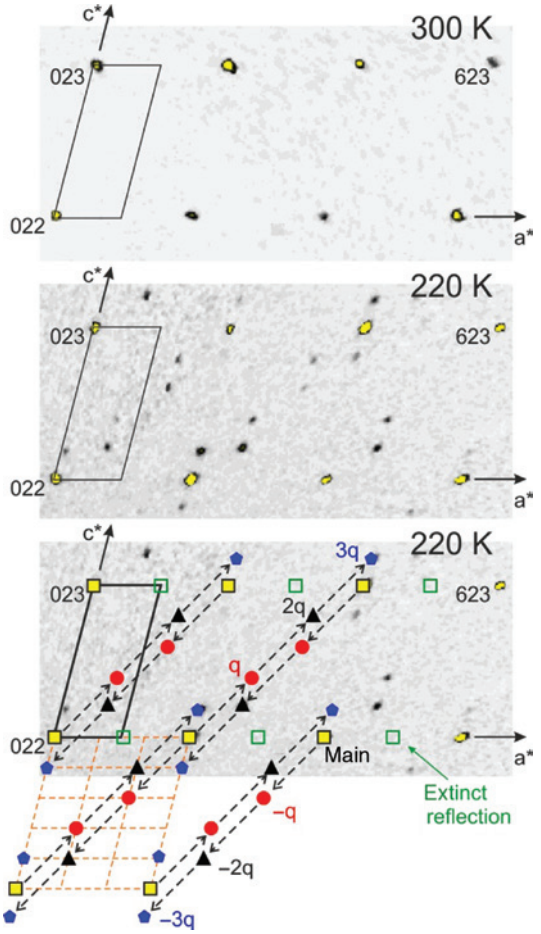

Fig. 3: Projection of a cutout of the reciprocal *h2l*–layer of CeCoAl at 300 and 220 K. The CeCoAl subcell at room temperature is drawn in black and some reflections are labeled; the positions of the extinct reflections due to the *C* centering are symbolized by green open squares. Black dashed arrows represent the *q*-vector ($q = 2/3, 0, 2/5$) for the (3+1) D modulated structure of CeCoAl below 271 K and the orange lines symbolize the supercell approximant (extinct reflections for 1/3a* are omitted). The main and the satellite reflections of the 1st, 2nd, and 3rd order are drawn as yellow squares, red circles, black triangles and blue pentagons, respectively. The intensity scale is based on (2 2 2) as the strongest reflection of the cutout. Yellow pixels are drawn with I > 1 %, black > 0.7 % and white 0 %.

the 3D supercell space group is present. Nevertheless, as already discussed above, a non-modulated 3D description with simple multiples of the axes could be realized, if all reflections of the $3a \times 5c$ approximant would be observed. Due to the systematic extinctions the (3+1)D modulated description has to be favored. The refinement of the $3a \times 5c$ superstructure lacks the necessary observations and could not be carried out.

As a consequence of the *a*15 transformation 15 independent crystallographic sites are realized for each atom type with systematic displacements off the ideal positions. The ideal positions are listed in Figure 5, while the observed ones are listed in Table 5. The most significant deviations can be observed for some of the Co-sites, which will be discussed later in the crystal structure part.

Beside the extensive data collections at 90, 180, 220 and 300 K, we additionally made an investigation of the intensity development in dependence of the temperature in the range from 220 to 300 K. For this measurement we

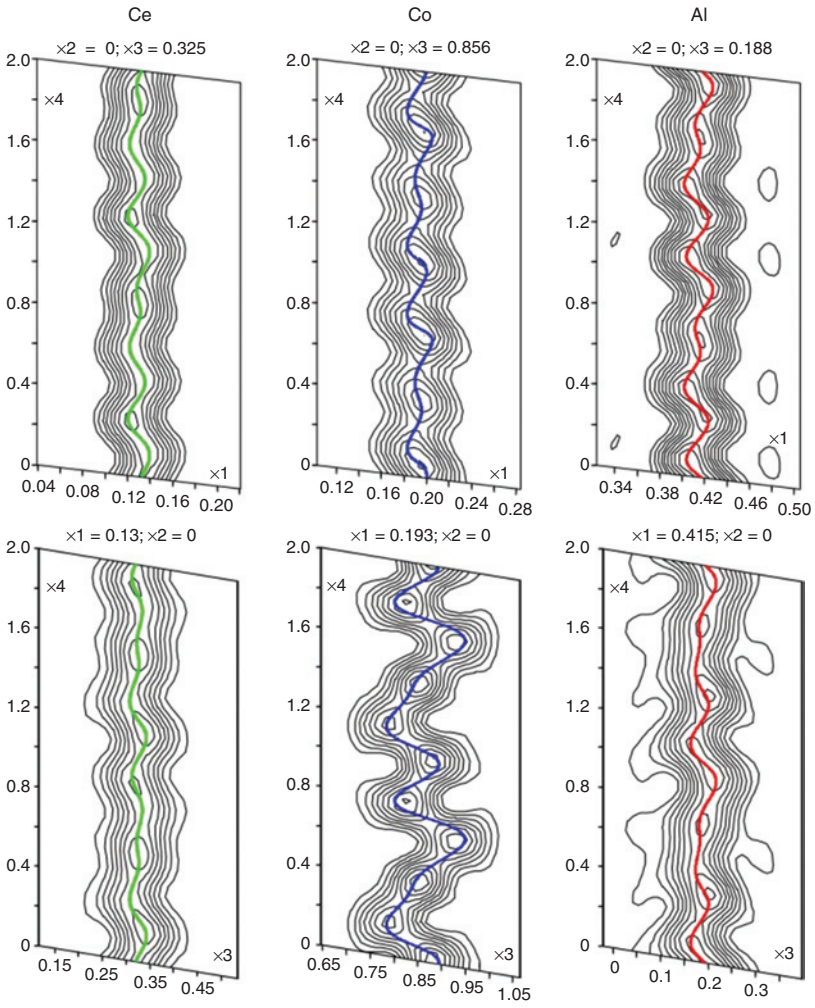

Fig. 4: Graphic representation of the atom domains of the commensurately modulated structure in x1 (top) and x3 (bottom) of CeCoAl at 90 K. For all atoms a harmonic position modulation has been realized. In all cases a summation of the projection directions has been applied (100 pm). Contour levels are > 0 with Δ = 12, 5 and 2 for Ce, Co and Al, respectively.

focus on the reflection (5.33 0 3.8), which is the 2nd order satellite of the (4 0 3) main reflection; called (4 0 3 2). The observed intensity was summed up in a defined detector image area and corrected by an average value for the background intensity. The calculated intensity as function of the temperature is displayed in Figure 6. A fit relating to the Landau theory failed [43]. Close to the phase transition the intensity extrapolates linearly to T_s of somewhat above 270 K. Taking the typical behavior that is expected from Landau theory into account this value would be too high. Another problem is the determination of the intensity due to the background, especially close to the phase transition. Consequently, the determination of the ordering temperature should in this case be done by physical property measurements.

Physical properties

In Figure 7 the temperature dependent heat capacity (left *y*-axis, black) as well as the inverse magnetic susceptibility (right *y*-axis, red) measured with an applied magnetic field of 10 kOe is depicted. The heat capacity clearly shows a λ-anomaly at T_S = 271(1) K identifying the structural phase transition as one of second order according to the classification of *Ehrenfest*. No additional phase transition, which could be related to a magnetic ordering, can be observed. Also the performed magnetic measurements give no hint for any magnetic ordering, which is totally in line with the significantly reduced magnetic moment. A mixed-valent character of CeCoAl could also be determined from X-ray absorption spectra (XAS) [11]. Almost at

Tab. 4: Atom positions, anisotropic displacement parameters (pm²) and Fourier coefficients of the modulation functions (sin, cos, × 10⁵) of CeCoAl at 90 K.

Atom	Wave	*x*	*y*	*z*	U_{11}	U_{22}	U_{33}	U_{13}	U_{eq}
Ce		0.12987(2)	0	0.32548(4)	97(1)	94(1)	89(1)	26(1)	93(1)
	sin(1)	101(6)	0	−184(14)	5(2)	2(3)	0(3)	3(2)	
	cos(1)	279(6)	0	293(14)	0(2)	0(3)	0(3)	0(2)	
	sin(2)	90(5)	0	847(15)	−4(2)	0(2)	−4(2)	3(1)	
	cos(2)	367(6)	0	−107(11)	−1(2)	1(2)	1(2)	2(1)	
	sin(3)	436(6)	0	661(15)	3(2)	0(2)	6(2)	4(1)	
	cos(3)	372(6)	0	−669(15)	1(1)	−7(2)	15(2)	2(1)	
Co		0.19331(4)	0	0.85590(17)	103(2)	95(2)	102(7)	19(3)	101(3)
	sin(1)	−248(13)	0	−319(4)	1(5)	−11(7)	39(7)	19(4)	
	cos(1)	−265(13)	0	−266(4)	−12(5)	−10(7)	−11(7)	−11(4)	
	sin(2)	241(12)	0	213(4)	2(4)	6(6)	39(5)	−3(4)	
	cos(2)	286(11)	0	378(4)	6(4)	−2(6)	14(7)	14(4)	
	sin(3)	−168(10)	0	−141(4)	−16(4)	−4(6)	−30(6)	−12(4)	
	cos(3)	702(12)	0	271(4)	−15(4)	1(6)	4(9)	0(5)	
Al		0.41459(10)	0	0.1884(3)	104(4)	104(3)	107(5)	29(4)	104(3)
	sin(1)	−214(29)	0	−535(76)	−12(11)	25(17)	2(16)	12(10)	
	cos(1)	375(30)	0	605(78)	−9(12)	12(17)	−1(16)	0(11)	
	sin(2)	−337(25)	0	−140(6)	8(10)	−9(13)	−1(11)	7(8)	
	cos(2)	−322(24)	0	−394(58)	13(10)	3(13)	−2(11)	5(9)	
	sin(3)	−769(23)	0	−1101(74)	−3(8)	2(13)	−6(13)	−13(8)	
	cos(3)	185(23)	0	289(73)	−12(9)	−12(16)	−7(14)	−17(9)	

All Wyckoff sites are 4*i*. U_{eq} is defined as one third of the trace of the orthogonalized U_{ij} tensor. Coefficients U_{ij} of the anisotropic displacement factor tensor of the atoms are defined by: $-2\pi^2[(ha^*)^2U_{11} + \ldots + 2hka^*b^*U_{12}]$. $U_{12} = U_{23} = 0$.

the same temperature of the λ-anomaly the inverse magnetic susceptibility shows an inflection point, confirming the phase transition at T_S = 271 K. This fits quite well to the temperature determined by measuring the intensity development of a satellite reflection. Furthermore two additional kinks can be observed at approximately 200 and 255 K for the χ^{-1} = f(T) data. These are most likely related to superparamagnetic Co-impurities that stick at grain boundaries.

The intermediate cerium valence behavior is obvious due to the absolute value of the inverse magnetic susceptibility. Nevertheless, it is not straightforward to determine an exact value for the cerium valence because of different difficulties. At first the Co-impurity hampers a correct fitting. Furthermore the best fitting procedure has to be chosen for a cerium compound with intermediate valence. The last point has already been discussed several times in literature [44–46]. In the case of CeCoAl a fitting with the ICF-model [44] leads to physical unrealistic values, consequently only Curie–Weiss fitting remains.

A magnetic measurement at higher fields (H = 25 kOe) shows less influence of the phase transition and the Co-impurity (not shown here). In the temperature range of 75–250 K the χ^{-1} data can be fitted using the Curie–Weiss law resulting in an effective magnetic moment of μ_{eff} = 1.62(5) μ_B/Ce atom, which is significantly below the free ion value of 2.54 μ_B for Ce^{3+}. This corresponds to the very short Ce–Co distance observed in the modulated structure (*vide infra*) (Table 6). A high negative value of θ_p = –98 K is observed for the Weiss constant which is typical for cerium compounds with intermediate valence. A further reason, but less important here might be crystal field splitting below 50 K. This clearly proves the intermediate cerium valence; however, the calculated magnetic moment should be interpreted carefully. A measurement of the magnetic susceptibility up to 350 K (not shown here) shows clearly a less steep increase of the inverse magnetic susceptibility above the phase transition. In accordance to the longer Ce–Co distance in the 3D structure this indicates a higher amount of trivalent cerium.

Future studies will focus on the synthesis of larger quantities of phase-pure CeCoAl for detailed physical property studies for comparison with the CeRuSn [18–29] data.

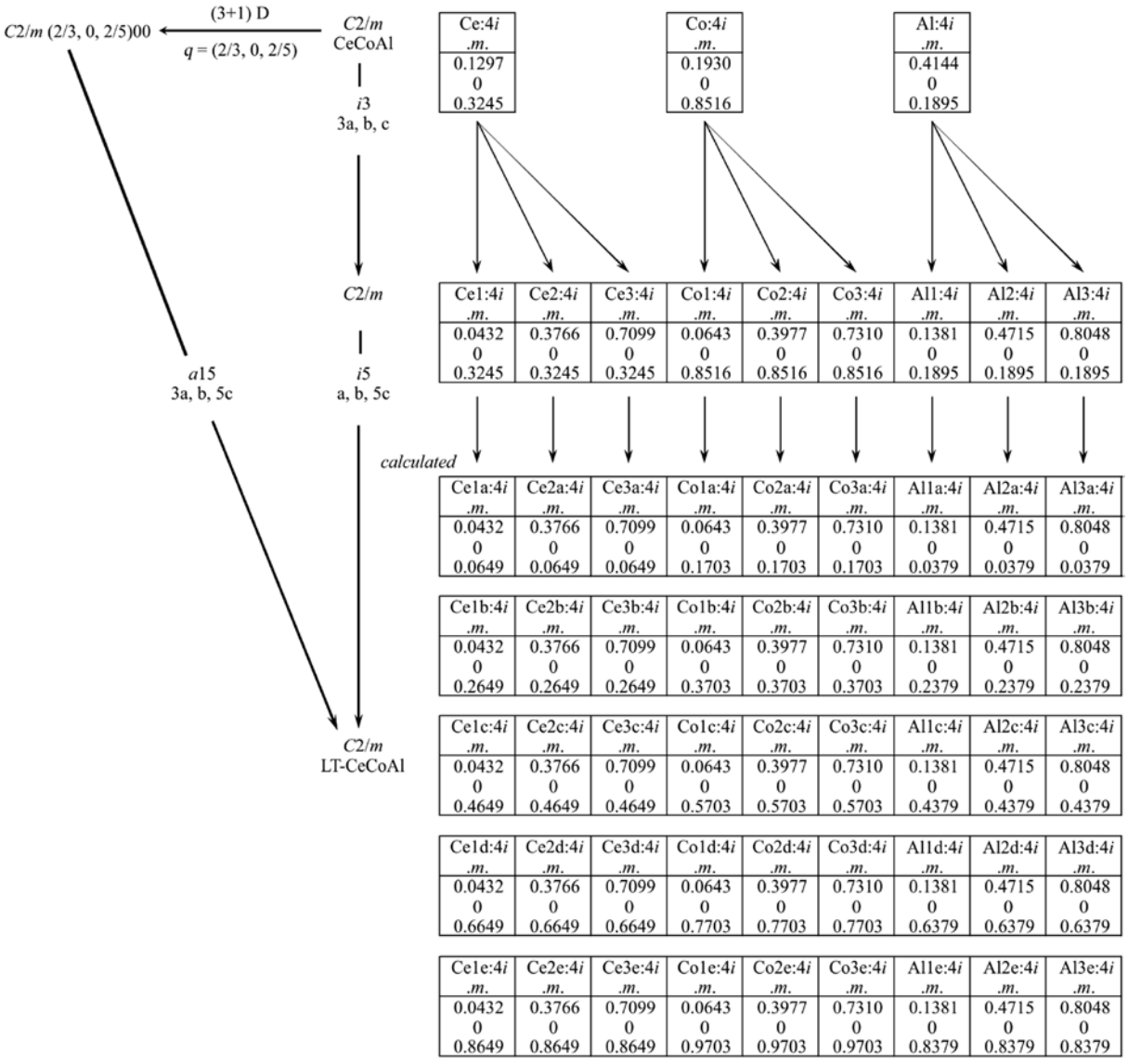

Fig. 5: Relation of the (3+1)D and 3D space groups of the modulated structure of CeCoAl and group-subgroup scheme in the Bärnighausen formalism [38–41] for the structures of CeCoAl at room and low temperatures (< 271 K). The indices for the *isomorphic* (*i*) symmetry reductions, the unit cell transformations, and the evolution of the atomic parameters are given. The index *a* is introduced for the formation of the approximant of the modulated structure as the product of the 3D *i* indices.

Crystal chemistry

At room temperature CeCoAl crystallizes in the monoclinic space group *C*2/*m* exhibiting its own structure type. Co- and Al-atoms build regular rhombs within the three dimensional [CoAl] network. The distances range from 249 to 257 pm (Table 3), which is only slightly above the sum of the covalent radii of 241 pm [47]. The Co–Co distances of 274.9 pm are well above the sum of the covalent radii of 232 pm. Furthermore very short distances can be observed between Ce and Co with 244.7 and 253.5 pm, which is significantly below the sum of the covalent radii of 281 pm [47]. This clearly confirms the mixed-valent character of cerium. The correlation of short distances and intermediate cerium valence has already extensively been described in literature for several Ce–Ru compounds [18–29].

Above the 271 K phase transition the Co-atoms displace irregularly off their equilibrium position, which is expressed by a slightly enlarged U_{33} anisotropic displacement parameter of the Co-atoms (cp. Figure 2, Table 2). This displacement becomes correlated along [3*a*, 0, 5*c*] in a rather complicated way at T_s. This is in contrast to

Tab. 5: Atom positions and anisotropic displacement parameters (pm²) of the $3a \times 5c$ approximant structure of CeCoAl at 90 K ($t_0 = 1/30$; $C2/m$, $a = 1107.5(1)$, $b = 440.3(1)$ and $c = 479.0(1)$ pm, $\beta = 104.7(1)°$).

Atom	*x*	*y*	*z*	U_{11}	U_{22}	U_{33}	U_{13}	U_{eq}
Ce1a	0.0409	0	0.0636	101	95	82	24	92
Ce1b	0.0408	0	0.2650	90	85	97	20	91
Ce1c	0.0459	0	0.4667	98	92	102	31	97
Ce1d	0.0452	0	0.6651	102	101	88	32	95
Ce1e	0.0436	0	0.8651	96	98	76	23	90
Ce2a	0.3762	0	0.0629	95	93	87	24	92
Ce2b	0.3739	0	0.2617	106	88	104	30	99
Ce2c	0.3756	0	0.4665	95	87	100	24	94
Ce2d	0.3799	0	0.6688	98	101	81	27	93
Ce2e	0.3776	0	0.8656	93	102	73	23	89
Ce3a	0.7084	0	0.0648	88	94	80	18	88
Ce3b	0.7104	0	0.2635	97	88	104	29	96
Ce3c	0.7098	0	0.4630	108	92	106	35	101
Ce3d	0.7105	0	0.6669	97	95	85	24	92
Ce3e	0.7108	0	0.8673	97	102	69	23	89
Co1a	0.0641	0	0.1793	137	103	126	44	120
Co1b	0.0638	0	0.3707	111	90	67	19	90
Co1c	0.0650	0	0.5645	97	88	126	38	102
Co1d	0.0665	0	0.7770	80	112	61	−18	90
Co1e	0.0628	0	0.9644	88	81	129	11	103
Co2a	0.3945	0	0.1573	112	85	154	21	119
Co2b	0.4002	0	0.3883	137	116	162	39	138
Co2c	0.3999	0	0.5788	91	86	103	25	93
Co2d	0.3983	0	0.7679	88	86	82	34	83
Co2e	0.3959	0	0.9637	85	101	9	−25	72
Co3a	0.7279	0	0.1615	107	94	20	−5	78
Co3b	0.7294	0	0.3591	116	89	160	35	122
Co3c	0.7352	0	0.5886	106	119	135	13	123
Co3d	0.7327	0	0.7754	76	82	115	15	93
Co3e	0.7303	0	0.9713	108	90	80	37	91
Al1a	0.1360	0	0.0372	88	115	100	10	104
Al1b	0.1382	0	0.2388	105	92	107	10	104
Al1c	0.1382	0	0.4359	99	133	119	63	110
Al1d	0.1386	0	0.6366	133	72	110	45	103
Al1e	0.1400	0	0.8399	96	106	100	18	101
Al2a	0.4692	0	0.0347	97	115	97	20	103
Al2b	0.4675	0	0.2351	121	115	106	33	113
Al2c	0.4745	0	0.4424	110	109	115	32	111
Al2d	0.4745	0	0.6397	82	123	117	50	103
Al2e	0.4720	0	0.8366	111	56	101	12	92
Al3a	0.8041	0	0.0366	100	66	98	−5	94
Al3b	0.8017	0	0.2329	104	129	107	45	110
Al3c	0.8027	0	0.4354	141	100	113	55	114
Al3d	0.8093	0	0.6435	104	109	111	32	107
Al3e	0.8065	0	0.8400	72	114	106	19	98

U_{eq} is defined as one third of the trace of the orthogonalized U_{ij} tensor. Coefficients U_{ij} of the anisotropic displacement factor tensor of the atoms are defined by: $-2\pi^2[(ha^*)^2U_{11}+\ldots+2hka^*b^*U_{12}]$. All Wyckoff sites are 4*i* and $U_{12} = U_{23} = 0$.

CeRuSn, where the modulations involve only the c^* direction. The basic unit cell of CeCoAl can be kept with a modulation vector of $q = 2/3\ a^* + 2/5\ c^*$. The superspace group $C2/m(\alpha 0 \gamma)00$ nicely resolves the "movement" of the Co-atoms from the ideal positions. Figure 8 shows the $3a \times 5c$ approximant for CeCoAl at 90 K and, additionally, the average Co-positions are marked by open circles. As a consequence of this distortion also the Ce- and Al-atoms move slightly away from their average positions, but less significantly. This behavior can also be understood by

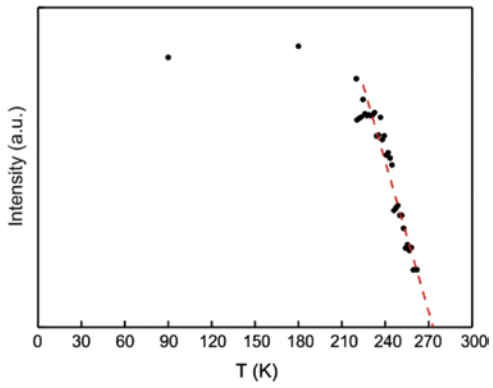

Fig. 6: Temperature dependency of the intensity of the 2nd order satellite (4 0 3 2).

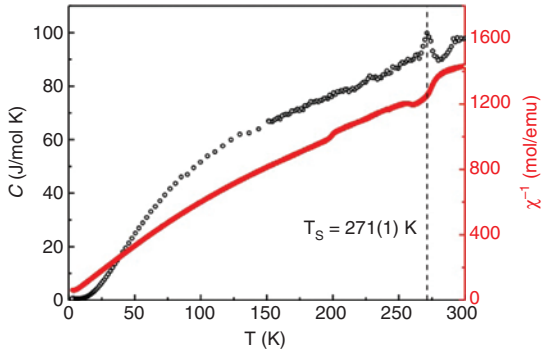

Fig. 7: Temperature dependent heat capacity (black circles) and inverse magnetic susceptibility (red circles) of CeCoAl. The heat capacity measurement was performed without an applied magnetic field, while for the magnetic susceptibility a field of 10 kOe was applied.

comparison of the calculated positions in Figure 5 with the observed ones in Table 5 or by reference to Figure 9. In this plot the displacements (top panel) as well as the distances in relation to Co (bottom panel) are plotted as a function of *t*. The dashed lines symbolize the commensurate *t* sections, which mark the realized displacements and distances in the $3a \times 5c$ approximant structure with $t_0 = 1/(2N) = 1/(2(3 \times 5)) = 1/30$ on a grid of $1/15 = 1/N = 1/(3 \times 5)$ projected onto the modulation functions with (3×5) as the least common multiple of the denominator of the *q*-vector components. On the basis of this plot it is obvious that the displacement of the Co-atoms along d*z* is significantly larger than for the other atoms and along d*x*, which is in line with the enlarged U_{33} ADP at 300 K. The largest deviations from the ideal positions concern Co2a, Co2b and Co3c (Figure 5).

The resulting Ce–Co interactions are most likely the propulsion of the phase transition and the resulting structural ordering scheme. In Figure 8 the shortest Ce–Co distances are highlighted by green and purple coloring and the corresponding distances are also marked in the *t*-plot. It is hardly surprising that the very short distances are related to the largest displacements of the Co-atoms from the average positions. The shortest Ce–Co distance in this structure is 218.8 pm (Ce2a–Co2a), which is even shorter than the Ce–Ru distances in $Ce_3Ru_2In_2$ (223 pm) [48] and CeRuSn (233 pm) [18]. Further distances of LT-CeCoAl are listed in Table 6. To our knowledge only for $Ce_3Co_4Al_4$ a Ce–Co distance below the sum of the covalent radii was reported so far [49]. Unfortunately, no investigation of the physical properties has been performed up to now for the latter compound.

Tab. 6: Interatomic distances (pm) for CeCoAl at 90 K (average, minimum, maximum) for the $3a \times 5c$ approximant. Standard deviations are equal or smaller than 1.0 pm.

Atom1	#	Atom2	d_{av}	d_{min}	d_{max}
Ce:	1	Co	245.9	218.8	293.5
	1	Co	252.3	222.5	275.5
	2	Al	318.9	316.1	322.5
	2	Co	321.4	314.9	333.4
	2	Al	324.6	322.4	328.8
	2	Al	333.2	331.1	338.2
	1	Al	338.0	329.7	347.9
	1	Co	347.0	343.2	353.3
	2	Ce	353.2	347.3	363.1
	1	Ce	366.9	364.0	370.7
	1	Ce	367.5	359.3	376.5
Co:	1	Ce	245.9	218.8	293.5
	2	Al	249.4	247.2	252.2
	1	Ce	252.3	222.5	275.5
	1	Al	256.8	247.9	265.8
	2	Co	273.0	267.7	276.4
	2	Ce	321.4	314.9	333.4
Al:	2	Co	249.4	247.2	252.2
	1	Co	256.8	247.9	265.8
	1	Al	292.8	290.1	296.1
	1	Al	310.4	295.4	330.6
	2	Ce	318.9	316.1	322.5
	2	Ce	324.6	322.4	328.8
	2	Ce	333.2	331.1	338.2
	1	Ce	338.0	329.7	347.9

In Table 5 all atomic displacement parameters (ADP) are listed for the $3a \times 5c$ approximant. Except two Co sites, no conspicuities can be observed for the ADPs. The U_{33} parameters of Co2e and Co3a are quite small leading to plate shaped probability of presences for these atoms. The corresponding modulations of the different ADPs for Co as a function of *t* are presented in Figure 10. The large minimum of the U_{33} around 0.3 is obvious in comparison to the other parameters. These anomalies for 2 of the 45 crystallographic sites point toward residual deficiencies

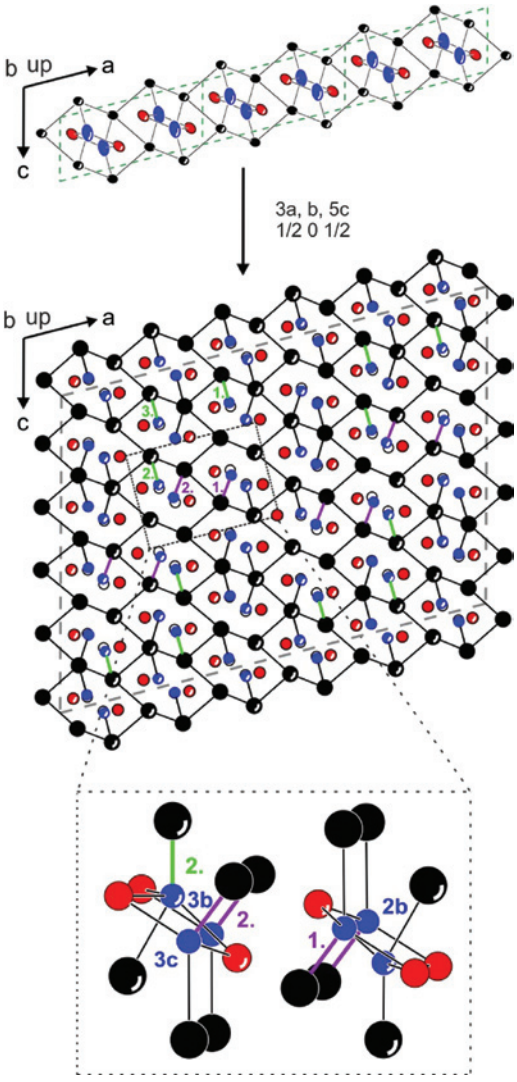

Fig. 8: Top part: Three unit cells of the CeCoAl subcell at 300 K (ellipsoids: 99 % probability); for comments see Figure 1. $3a \times 5c$ approximant structure of CeCoAl at 90 K (middle part). In the bottom part a cutout with a slightly tilted *b*-axis is presented. Emphasized Ce–Co distances are 221.6, 223.2 and 222.5 for green 2, purple 2 and purple 1, respectively. Cerium, cobalt and aluminum atoms are drawn as black, blue, and red circles, respectively. The crescents mark the atoms with $y = 1/2$. To emphasize the position modulation of Co the ideal Co positions are symbolized by open circles. The shortest Ce–Co distances are highlighted in green and purple, these distances are additionally marked in the *t*-plot (cp. Figure 8).

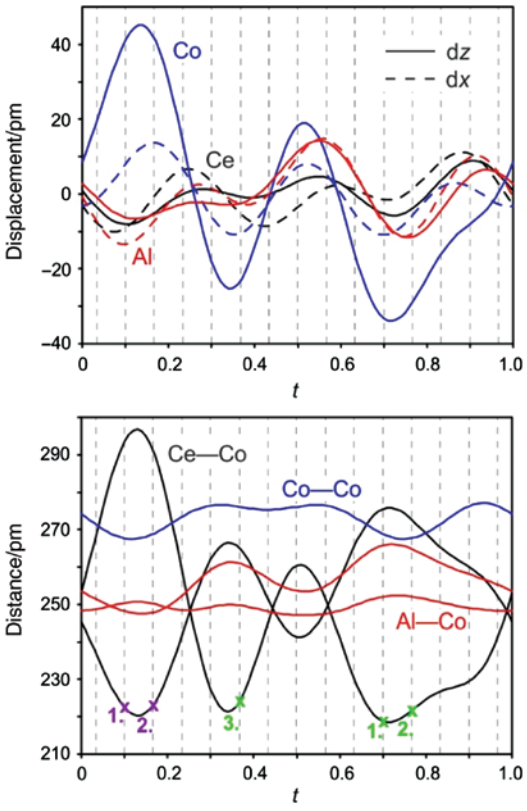

Fig. 9: Displacement (top) and distance (bottom) modulations as a function of *t*. Black, blue and red lines represent Ce, Co and Al, respectively. The dashed lines indicate the commensurate *t* sections with $t_0 = 1/30$. Green and purple crosses mark the shortest Ce–Co distances corresponding to Figure 7.

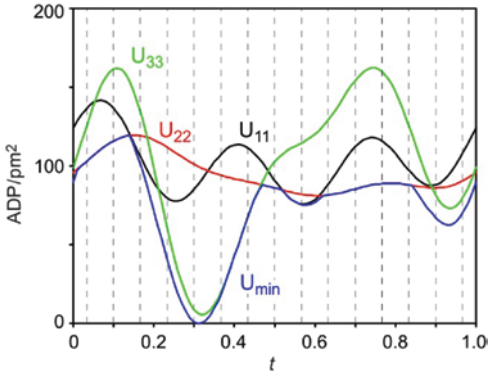

Fig. 10: Atomic displacement parameter (ADP) modulations of Co as a function of *t*. The dashed lines indicate the commensurate *t* sections with $t_0 = 1/30$.

of the refined modulation rather than object the presented structure description.

Up to now the temperature dependency of the modulation has not been discussed. In Figure 11 the modulation of the Ce–Co distances in dependence of *t* has been plotted for the three different temperatures (90, 180 and 220 K) below the phase transition. At first it has to be noted that the modulations for all temperatures are basically the same. Nevertheless, it is obvious that the 90 and 180 K curves are almost identical, while the 220 K one exhibits small differences, which is totally in line with the Landau theory.

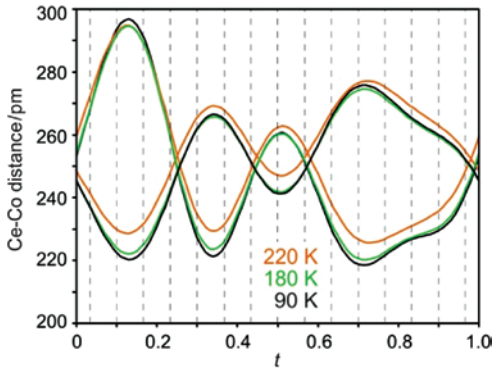

Fig. 11: Ce–Co distance modulations as a function of t for 90 (black), 180 (green) and 220 K (orange). The dashed lines indicate the commensurate t sections with $t_0 = 1/30$.

Conclusively, we would like to discuss how the introduced modulation influences the structure and for this we refer to Figure 12. In this plot the symmetry thinning by a factor of 15 from the structure at 300 K to the approximant structure at 90 K is symbolized. The top panel shows the projection of the $3a \times 5c$ approximant along the monoclinic axis. Like already discussed above, symmetry thinning leads mainly to a displacement of the Co-atoms from the ideal position which is forced by the interactions between Ce and Co. Consequently, the 15 shortest Ce–Co distances are drawn in this figure. By numbering of these distances a coloring could be established, whereby same colors but different patterns are related by an inversion center. Due to the coloring the remaining symmetry elements and the multiples of the a- and c-axis can be easily identified. For the last point it has to be taken into account that one half of the drawn atoms are at $y = 1/2$, which are marked by crescents.

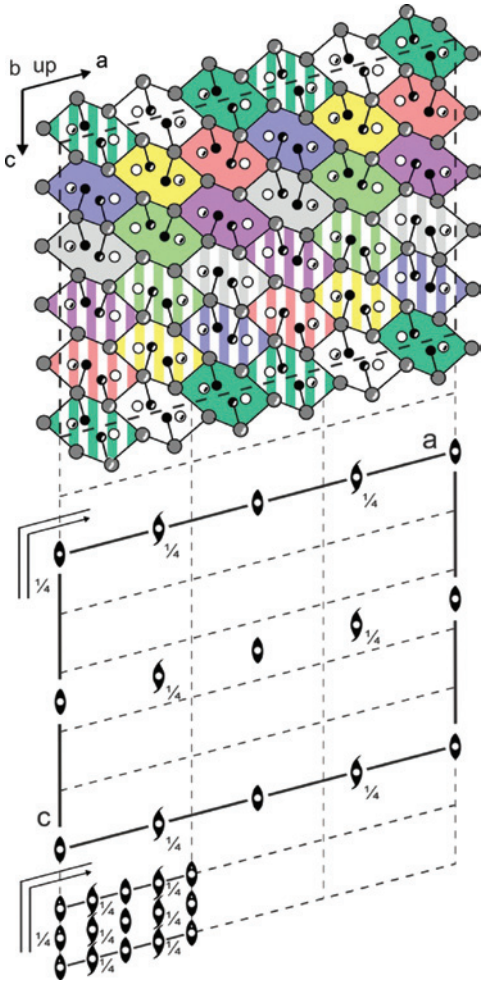

Fig. 12: Symmetry element thinning from the subcell at 300 K (bottom) to the $3a \times 5c$ approximant structure of CeCoAl at 90 K (middle and top). The black dashed lines symbolize the lattice of the subcell and the crescents mark the atoms with $y = 1/2$. In the top part the 15 shortest Ce–Co distances are drawn and the coloration symbolizes the arrangement of these. Areas with same colors but different pattern (filled and striped) are related by an inversion center.

Conclusion

The structure of CeCoAl at low temperatures can be described in the (3+1)D space group $C2/m(\alpha 0 \gamma)00$ with $q = (2/3, 0, 2/5)$, while at ambient conditions the monoclinic 3D space group $C2/m$ is present. The phase transition of $T_S = 271$ K could be determined best by investigation of the heat capacity. This phase transition is most likely forced by interactions between Co and Ce. In the approximant of the modulated structure very short distances (218.8 pm Ce–Co) far below the sum of the covalent radii can be observed. These short distances can only be explained by partly tetravalent cerium. Such a behavior is already known for different intermetallics containing cerium and ruthenium, like CeRuSn, which has the same valence electron count as CeCoAl. CeCoGa, subject of an upcoming paper, with another peculiar modulation fits nicely in the here discussed scheme.

Acknowledgments: This work was supported by the Deutsche Forschungsgemeinschaft. O. N. is indebted to the NRW Forschungsschule *Molecules and Materials – A Common Design Principle* for a PhD fellowship.

References

[1] A. Szytuła, J. Leciejewicz, *Handbook of Crystal Structures and Magnetic Properties of Rare Earth Intermetallics*, CRC Press, Boca Raton, **1994**.

[2] S. F. Matar. *Progr. Solid State Chem*. **2013**, *41*, 55.
[3] P. Villars, K. Cenzual, *Pearson's Crystal Data: Crystal Structure Database for Inorganic Compounds (release 2014/15)*, ASM International®, Materials Park, Ohio (USA) **2014**.
[4] S. Gupta, K. G. Suresh. *J. Alloys Compd*. **2015**, *618*, 562.
[5] R. Pöttgen, B. Chevalier. *Z. Naturforsch*. **2015**, *70b*, 289.
[6] O. S. Zarechnyuk, R. M. Ryjkal', V. V. Korin. *Dopov. Akad. Nauk Ukr. RSR, Ser. A* **1980**, 86.
[7] Yu. N. Grin', O. M. Sichevich, V. A. Bruskov, R. M. Rykhal', Ya. P. Yarmolyuk. *Sov. Phys. Crystallogr*. **1983**, *28*, 346.
[8] M. E. Kost, A. L. Shilov. *Izv. Akad. Nauk SSSR* **1983**, 7.
[9] A. L. Shilov. *Russ. J. Phys. Chem*. **1987**, *61*, 719.
[10] M. D. Koterlin, B. S. Morokhivski, Yu. N. Grin, O. M. Sichevich. *Dopov. Akad. Nauk Ukr. RSR, Ser. A* **1988**, 11, 70.
[11] M. D. Koterlyn, B. S. Morokhivski, I. D. Shcherba, L. J. Živković, R. V. Lutsiv. *J. Serb. Chem. Soc*. **1991**, *56*, 733.
[12] M. C. Gao, N. Ünlü, M. Mihalkovic, M. Widom, G. J. Shiflet. *Met. Mater. Trans. A* **2007**, *38A*, 2540.
[13] Q. Yao, H. Zhou, C. Tang, S. Pan. *J. Rare Earths* **2011**, *29*, 650.
[14] N. Nasri, J. Gastebois, M. Pasturel, B. Belgacem, I. Péron, F. Gouttefangeas, R. Ben Hassen, O. Tougait, H. Noël. *J. Alloys Compd*. **2015**, *628*, 277.
[15] V. A. Romaka, O. M. Sichevich, R. E. Gladyshevskiy, Ya. P. Yarmolyuk, Yu. N. Grin. *Phys. Met. Metall.* **1983**, *56*, 53.
[16] B. Chevalier, J.-L. Bobet, M. Pasturel, E. Gaudin, J. Etourneau. *J. Alloys Compd*. **2003**, *356–357*, 147.
[17] J. Goraus, A. Ślebarski, M. Fijałkowski. *Intermetallics* **2013**, *32*, 219.
[18] J. F. Riecken, W. Hermes, B. Chevalier, R.-D. Hoffmann, F. M. Schappacher, R. Pöttgen. *Z. Anorg. Allg. Chem*. **2007**, *633*, 1094.
[19] S. F. Matar, J. F. Riecken, B. Chevalier, R. Pöttgen, A. F. Al Alam, V. Eyert. *Phys. Rev. B* **2007**, *76*, 174434.
[20] J. Mydosh, A. M. Strydom, M. Baenitz, B. Chevalier, W. Hermes, R. Pöttgen. *Phys. Rev. B* **2011**, *83*, 054411.
[21] F. M. Schappacher, P. Khuntia, A. K. Rajarajan, M. Baenitz, J. A. Mydosh, B. Chevalier, S. F. Matar, R. Pöttgen. *Z. Naturforsch*. **2012**, *67b*, 473.
[22] K. Prokeš, J. Mydosh, O. Prokhnenko, W.-D. Stein, S. Landsgesell, W. Hermes, R. Feyerherm, R. Pöttgen. *Phys. Rev. B* **2013**, *87*, 094421.
[23] J. Fikáček, J. Prchal, J. Prokleška, I. Císařová, V. Sechovský. *Solid State Phen*. **2013**, *194*, 40.
[24] J. Fikáček, J. Prokleška, J. Prchal, J. Custers, V. Sechovský. *J. Phys.: Condens. Matter* **2013**, *25*, 416006.
[25] V. Gribanova, E. Murashova, Yu. Seropegin, A. Gribanov. *J. Alloys Compd*. **2014**, *585*, 352.
[26] K. Prokeš, V. Petříček, E. Ressouche, S. Hartwig, B. Ouladdiaf, J. A. Mydosh, R.-D. Hoffmann, Y.-K. Huang, R. Pöttgen. *J. Phys.: Condens. Matter* **2014**, *26*, 122201.
[27] K. Prokeš, S. A. J. Kimber, J. A. Mydosh, R. Pöttgen. *Phys. Rev. B* **2014**, *89*, 064106.
[28] R. Feyerherm, E. Dudzik, K. Prokeš, J. A. Mydosh, Y.-K. Huang, R. Pöttgen. *Phys. Rev. B* **2014**, *90*, 041104.
[29] K. Prokeš, S. Hartwig, A. Gukasov, J. A. Mydosh, Y.-K. Huang, O. Niehaus, R. Pöttgen. *Phys. Rev. B* **2015**, *91*, 014424.
[30] N. N. Zhuravlev. *Sov. Phys. JETP* **1957**, *5*, 1064.
[31] L. J. Cabri, D. C. Harris, R. I. Gait. *Can. Mineral*. **1973**, *11*, 903.
[32] M. Heise, J.-H. Chang, R. Schönemann, T. Herrmannsdörfer, J. Wosnitza, M. Ruck. *Chem. Mater*. **2014**, *26*, 5640.
[33] R. Pöttgen, Th. Gulden, A. Simon. *GIT Labor-Fachzeitschrift* **1999**, *43*, 133.
[34] R. Pöttgen, A. Lang, R.-D. Hoffmann, B. Künnen, G. Kotzyba, R. Müllmann, B. D. Mosel, C. Rosenhahn. *Z. Kristallogr.* **1999**, *214*, 143.
[35] K. Yvon, W. Jeitschko, E. Parthé. *J. Appl. Crystallogr*. **1977**, *10*, 73.
[36] L. Palatinus, G. Chapuis. *J. Appl. Crystallogr.* **2007**, *40*, 786.
[37] V. Petříček, M. Dušek, L. Palatinus. *Z. Kristallogr.* **2014**, *229*, 345.
[38] H. Bärnighausen. *Commun. Math. Chem*. **1980**, *9*, 139.
[39] U. Müller. *Z. Anorg. Allg. Chem*. **2004**, *630*, 1519.
[40] U. Müller, in *Relating Crystal Structures by Group-Subgroup Relations*, (Eds. H. Wondratschek and U. Müller) *International Tables for Crystallography*, Vol. A1, *Symmetry relations between space groups*, John Wiley & sons, Ltd, 2nd Ed., Chichester, pp. 44–56, **2010**.
[41] U. Müller, *Symmetriebeziehungen zwischen verwandten Kristallstrukturen*, Vieweg + Teubner Verlag, Wiesbaden, **2012**.
[42] C. Schwickert, R.-D. Hoffmann, F. Winter, R. Pöttgen. *Z. Kristallogr.* **2014**, *229*, 525.
[43] L. Landau. *Ukr. J. Phys*. **2008**, *53*, 25.
[44] O. Niehaus, P. M. Abdala, R. Pöttgen. *Z. Naturforsch.* **2015**, *70b*, 253.
[45] O. Niehaus, P. M. Abdala, J. F. Riecken, F. Winter, B. Chevalier, R. Pöttgen. *Z. Naturforsch.* **2013**, *68b*, 960.
[46] O. Niehaus, P. M. Abdala, R. St. Touzani, B. P. T. Fokwa, R. Pöttgen. *Solid State Sci.*, **2015**, *40*, 36.
[47] J. Emsley. *The Elements*, Oxford University Press, Oxford (U.K.) **1999**.
[48] A. I. Tursina, Zh. M. Kurenbaeva, A. V. Gribanov, H. Noël, T. Roisnel, Y. D. Seropegin. *J. Alloys Compd*. **2007**, *442*, 100.
[49] G. Cordier, G. Dörsam, R. Kniep. *J. Magn. Magn. Mater.* **1988**, *76–77*, 653.